

Cite this: *Chem. Sci.*, 2012, **3**, 1024

www.rsc.org/chemicalscience

EDGE ARTICLE

Direct observation of a ferri-to-ferromagnetic transition in a fluoride-bridged 3d–4f molecular cluster†

Jan Dreiser,^{*a} Kasper S. Pedersen,^{*b} Cinthia Piamonteze,^a Stefano Rusponi,^c Zaher Salman,^d Md. Ehesan Ali,^e Magnus Schau-Magnussen,^b Christian Aa. Thuesen,^b Stergios Piligkos,^b Høgni Weihe,^b Hannu Mutka,^f Oliver Waldmann,^g Peter Oppeneer,^h Jesper Bendix,^{*b} Frithjof Nolting^a and Harald Brune^c

Received 13th October 2011, Accepted 6th December 2011

DOI: 10.1039/c2sc00794k

We report on the synthesis, crystal structure and magnetic characterisation of the trinuclear, fluoride-bridged, molecular nanomagnet [Dy(hfac)₃(H₂O)–CrF₂(py)₄–Dy(hfac)₃(NO₃)] (**1**) (hfacH = 1,1,1,5,5,5-hexafluoroacetylacetone, py = pyridine) and a closely related dinuclear species [Dy(hfac)₄–CrF₂(py)₄]^{1/2}·1/2 CHCl₃ (**2**). Element-specific magnetisation curves obtained on **1** by X-ray magnetic circular dichroism (XMCD) allow us to directly observe the field-induced transition from a *ferromagnetic* to a *ferri*magnetic arrangement of the Dy and Cr magnetic moments. By fitting a spin-Hamiltonian model to the XMCD data we extract a weak antiferromagnetic exchange coupling of $j = -0.18 \text{ cm}^{-1}$ between the Dy^{III} and Cr^{III} ions. The value found from XMCD is consistent with SQUID magnetometry and inelastic neutron scattering measurements. Furthermore, alternating current susceptibility and muon-spin relaxation measurements reveal that **1** shows thermally activated relaxation of magnetisation with a small effective barrier for magnetisation reversal of $\Delta_{\text{eff}} = 3 \text{ cm}^{-1}$. Density-functional theory calculations show that the Dy–Cr couplings originate from superexchange *via* the fluoride bridges.

Introduction

Lanthanides are promising building blocks for molecular magnetic materials: incorporating 4f ions in molecular clusters to form single-molecule magnets¹ (SMMs) is of high interest as 4f metals exhibit stronger spin–orbit coupling than their 3d counterparts and most of them possess a ground state characterised

by an unquenched orbital momentum. The ligand-field splittings of the ground multiplet are typically on the order of the thermal energy at room temperature and result in large energy barriers for magnetisation reversal which are an important prerequisite to achieve long magnetisation-relaxation times.² This is especially well exemplified by mononuclear phthalocyaninate,³ polyoxometalate,⁴ organometallic⁵ or purely inorganic⁶ lanthanide compounds, all shown to exhibit SMM behaviour. Very recently, significant advances in the synthesis of polynuclear 4f clusters such as the achievements of record-high energy barriers up to $\sim 530 \text{ K}^7$ and of a strong exchange coupling *via* a N₂³⁻ radical bridge⁸ have been reported. Also, slow relaxation in some 3d–4f clusters⁹ has recently been realised at temperatures comparable to those for 3d-only SMMs.

Understanding the magnetic behaviour of 4f-containing clusters is much more challenging than that of 3d-only systems. Determining the ligand-field parameters of 4f ions requires extensive studies, and the extraction of spin-Hamiltonian parameters such as intracluster magnetic exchange coupling can be tricky. In 3d clusters this information can in most cases be readily obtained from direct current (dc) magnetic susceptibility, while in the case of 4f it is often buried under the dominant effect of ligand-field splittings.¹⁰ Not even the m_J of the ground-state can be taken for granted, as it depends on the exact ligand field.¹¹ To this end, X-ray magnetic circular dichroism^{12,13} (XMCD) can provide clear-cut information and thus help in the

^aSwiss Light Source, Paul Scherrer Institut, CH-5232 Villigen PSI, Switzerland. E-mail: jan.dreiser@psi.ch

^bDepartment of Chemistry, University of Copenhagen, DK-2100 Copenhagen, Denmark. E-mail: ksp@kiku.dk; bendix@kiku.dk

^cInstitute of Condensed Matter Physics, Ecole Polytechnique Fédérale de Lausanne, CH-1015 Lausanne, Switzerland

^dLaboratory for Muon Spin Spectroscopy, Paul Scherrer Institut, CH-5232 Villigen PSI, Switzerland

^eCenter for Theoretical Chemistry, Ruhr-Universität Bochum, D-44801 Bochum, Germany

^fInstitut Laue-Langevin, F-38042 Grenoble Cedex 9, France

^gPhysikalisches Institut, Universität Freiburg, D-79104 Freiburg, Germany

^hDepartment of Physics and Astronomy, Uppsala University, Box 516, S-751 20 Uppsala, Sweden

† Electronic supplementary information (ESI) available: experimental section; thermal ellipsoid plots; XMCD sum rules analysis; details of ligand-field multiplet calculations; additional SQUID measurements on **1**; SQUID measurements on **2** and their analysis; analysis of the INS data and of the μ SR measurements; details of the spin-Hamiltonian models; details of the DFT calculations. CCDC reference numbers 848193–848194. For ESI and crystallographic data in CIF or other electronic format see DOI: 10.1039/c2sc00794k

characterisation of 3d–4f compounds. Its main strength is the ability for measuring spin and orbital magnetic moments with elemental selectivity and ultrahigh sensitivity reaching down to submonolayers.

Here, we use XMCD to obtain element-specific magnetisation curves for the Dy^{III} and Cr^{III} ions in a novel type fluoride-bridged Dy^{III}–Cr^{III}–Dy^{III} cluster. Our data provide direct evidence for the field-induced transition from a ferrimagnetic to a ferromagnetic configuration of the magnetic moments in this trinuclear compound. This effect is manifested by a wiggle shape observed in the magnetisation curve of the Cr^{III} ion. Using spin-Hamiltonian models we are able to quantify the strength of the magnetic exchange coupling between Dy^{III} and Cr^{III} ions.

The vast majority of 4f¹⁴ and mixed 3d–4f clusters are bridged by oxide,¹⁵ hydroxide^{14a} or alkoxides.^{2c,9} Here, we have been pursuing the possibilities of utilizing fluoride bridges—an approach which is nearly without precedence. This is intriguing as the fluoride ion proffers low basicity and a preference for pseudo-linear bridging, the latter facilitating prediction and design of specific molecular cluster topologies.¹⁶ The synthesis of fluoride-bridged 3d–4f SMMs is obviously complicated due to the possible formation of insoluble lanthanide(III) fluoride. Nevertheless a few examples of fluoride-bridged 3d–4f clusters incorporating diamagnetic Ti^{IV} have been prepared by serendipitous approaches. The scarce examples include only [La{(C₅Me₄Et)₂Ti₂F₇}₃] and [Ln{(C₅Me₅)₂Ti₂F₇}₃] (Ln = Pr, Nd)^{17,18} in which the 12-coordinate lanthanide ion is exclusively surrounded by fluoride ions. Recently the first clusters incorporating {Cr^{III}–F–Ln^{III}} linking units were reported by Winpenny and co-workers.¹⁹ The authors showed that reaction of a {Cr₆} horseshoe [(R₂NH₂)₃{Cr₆F₁₁(O₂C^tBu)₁₀}₂] (R = Et, ⁿPr) with dinuclear [Ln(O₂C^tBu)₃(HO₂C^tBu)₃]₂ yields mixed 3d–4f clusters with metal ion stoichiometries of {CeCr₆}, {Gd₂Cr₆} and {Ln₄Cr₁₂}. However, in all of these, the {Cr^{III}–F–Ln^{III}} units are further supported by carboxylate bridging. Some of us recently reported the first examples of Cr^{III}–Ln^{III} clusters containing unsupported {Cr–F–Ln} bridges.²⁰ The synthetic principle is based on the kinetic robustness of octahedral Cr^{III} complexes which suppresses the tendency of fluoride abstraction by the lanthanide ion.²¹ Employment of another precursor; the *trans*-difluorido complex, *trans*-[CrF₂(py)₄]NO₃, has the advantage of being both robust and soluble in non-coordinating solvents such as chloroform.

In this work, we present a multi-technique study and the syntheses and structures of two fluoride-bridged Cr^{III}–Dy^{III} complexes: a trinuclear [Dy(hfac)₃(H₂O)–CrF₂(py)₄–Dy(hfac)₃(NO₃)] (**1**) (hfacH = 1,1,1,5,5,5-hexafluoroacetyl-acetone, py = pyridine) and a dinuclear species [Dy(hfac)₄–CrF₂(py)₄]^{1/2} CHCl₃ (**2**).

Results

Synthesis and structural analysis

Both **1** and **2** are obtained by the coordination of *trans*-[CrF₂(py)₄]⁺ to [Dy(hfac)₃(H₂O)₂] in chloroform solution. For the preparation of **1**, a large excess of [Dy(hfac)₃(H₂O)₂] is needed to avoid precipitation of **2**. By using four equivalents of [Dy(hfac)₃(H₂O)₂], pink needles of a trinuclear, fluoride-bridged asymmetric [Dy(hfac)₃(H₂O)–CrF₂(py)₄–Dy(hfac)₃(NO₃)] cluster (**1**) result. The

structures of **1** and **2** are depicted in Fig. 1, thermal-ellipsoid plots are shown in Figs. S1 and S2 (ESI†). **1** crystallises in the monoclinic space group *C2/c*. The coordination sphere of Dy(1) consists of three, bidentate hfac[−] ligands and one bidentate nitrate ion which is engaged in hydrogen bonding to a water molecule coordinated at Dy(3) in a neighbouring molecule. The central Cr^{III} ion is located on a crystallographic two-fold axis leading to systematic disorder of the water and nitrate coordinated to Dy. The Cr–F distance is 1.903(2) Å which is longer than the value found in the *trans*-[CrF₂(py)₄]PF₆ complex (Cr–F = 1.853(2) Å).²² The pyridine ligands coordinated to Cr^{III} are arranged with a twist of approximately 30° following the twist of the hfac[−] ligands.

On the other hand, reaction of one-to-one stoichiometry yields red-violet, block-shaped crystals of [Dy(hfac)₄–CrF₂(py)₄]^{1/2} CHCl₃ (**2**). **2** crystallises in the triclinic space group *P1̄* and contains an almost linear Cr–F–Dy bridge (177.74(7)°) between a {Cr^{III}F₂(py)₄}⁺ and a {Dy(hfac)₄}[−] unit. The Cr^{III} ion is octahedrally coordinated whereas the 9-coordinate Dy^{III} can be described as tri-capped trigonal prismatic. The four bidentate hfac[−] ligands coordinated to Dy create a four-bladed propeller twist. The asymmetric unit contains both the Δ- and Λ-isomer of [Dy(hfac)₄–CrF₂(py)₄]. The Cr–F bond lengths of the bridging fluorides are significantly elongated (1.9145(14) Å and 1.9045(14) Å) compared to the non-bridging fluorides (1.8440(15) Å and 1.8416(15) Å). The Dy–F distances (2.3474(15) Å and 2.3245(14) Å) are shorter than the Dy–O bond lengths which are in the range 2.3689(18) Å to 2.4496(19) Å.

X-ray magnetic circular dichroism

Polarisation-dependent X-ray absorption spectra of **1** are shown in Fig. 2a and 3a. The spectra were taken at the Dy M_{4,5} and the

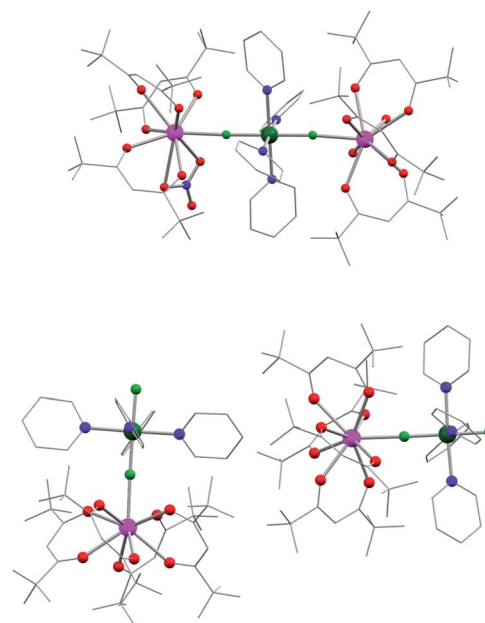


Fig. 1 Molecular structure of **1** (top) and **2** (bottom, both molecules in the asymmetric unit are shown) as obtained from X-ray diffraction. Color code: pink: Dy, dark green: Cr, light green: F, red: O, blue: N. Carbon skeletons and non-bridging fluorines are shown as wireframe and hydrogens and solvent molecule in **2** are omitted for clarity.

Cr $L_{2,3}$ edges at the indicated magnetic fields and temperatures. Clearly, the observed spectra of both Dy^{III} and Cr^{III} ions are strongly dichroic. Fig. 2c and 3c show the resulting XMCD spectra for the respective elements. While the XMCD of Dy is almost saturated at $B = 1$ T, this is not the case for Cr: here the XMCD signature flips its sign upon increasing the field from 1 T to 6 T corresponding to a field-induced flip of the Cr magnetic moment. This behaviour is also reflected in the element-specific magnetisation curves shown in Fig. 4a and 4b. Curve (a) is indicative for the Cr moment being antiparallel to the field at small, and parallel to it at large external field, while curve (b) indicates that the Dy moments behave similar to paramagnets with a saturation field around 2 T at 2 K. The data show some similarities to those recently observed on $TbPc_2$ molecules coupled to a ferromagnetic substrate.¹³ⁿ However, the curves on **1** are fully reversible without hysteresis. Black squares indicate the total (spin and orbital) Dy magnetic moments extracted from the XMCD spectra using sum rules²³ (for details see ESI†). Note that these moments represent the average over the two nonequivalent Dy sites in the trinuclear cluster because XMCD is element selective but not site selective.

The obtained ratio of $\langle L_z \rangle / \langle S_z \rangle$ is 1.9(4) for Dy, in excellent agreement with the value of 2.0 derived from Hund's rules. In the Cr case, the sum rules are not applicable because of the small energy separation between the Cr L_2 and L_3 edges.²⁴ Here, the absolute values of the Cr magnetic moments were extracted using ligand-field multiplet calculations (see ESI†).

SQUID magnetometry

Fig. 4c shows the cluster magnetisation curve of **1** obtained by SQUID magnetometry at 1.9 K. After a steep rise near zero field the slope reduces upon increasing the field but no clear saturation can be observed, suggesting strong anisotropy and/or the presence of low-energy excited states.

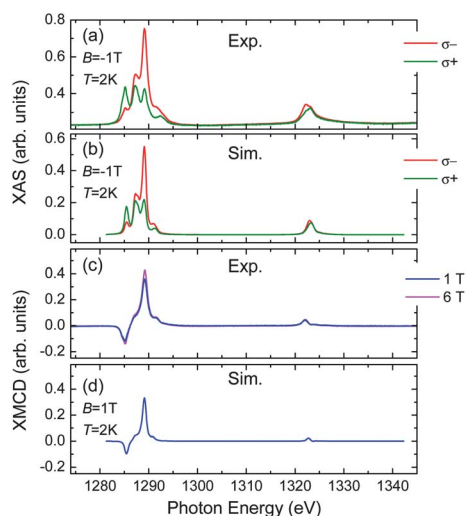


Fig. 2 (a) X-ray absorption spectra of **1** at the Dy $M_{4,5}$ edges recorded for two photon helicities at the indicated magnetic field and temperature. (b) X-ray absorption spectra obtained from ligand-field multiplet calculations. (c) XMCD spectra measured on **1** at different magnetic fields and $T = 2$ K. (d) Simulated XMCD spectrum. See ESI† for parameters of simulations (b) and (d).

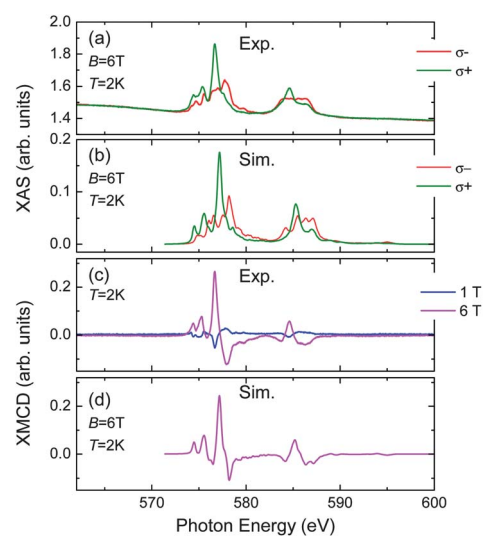


Fig. 3 (a) X-ray absorption spectra of **1** at the Cr $L_{2,3}$ edges recorded for two photon helicities at the indicated magnetic field and temperature. (b) X-ray absorption spectra obtained from ligand-field multiplet calculations. (c) XMCD spectra measured on **1** at different magnetic fields and $T = 2$ K. (d) Calculated XMCD spectrum. The simulation parameters for (b) and (d) are given in the ESI†.

Fig. 5 depicts the temperature dependence of the dc magnetic susceptibility of **1** represented as the χT product. When decreasing the temperature from 300 K, the susceptibility initially drops moderately. Upon further decrease the curve bends downwards and goes through a minimum at 4 K. In 3d-only transition-metal clusters with a magnetic ground state, this behaviour would indicate intramolecular antiferromagnetic interactions. However, this argument may fail for clusters containing 4f ions due to the orbital contribution to their magnetism.¹⁰ The room-temperature value is $\chi T = 30.15 \text{ cm}^3 \text{ K mol}^{-1}$ yielding perfect agreement with the value expected for two isolated Dy^{III} ions with $g_J = 4/3$ and a Cr^{III} ion with $g_S = 2$.

In the out-of-phase component of the ac susceptibility of **1**, a clearly frequency-dependent onset of a peak is observed within the accessible temperature ($T \geq 1.8$ K) and frequency (0.1–1500 Hz) range, as shown in Fig. 6a. This behaviour combined with

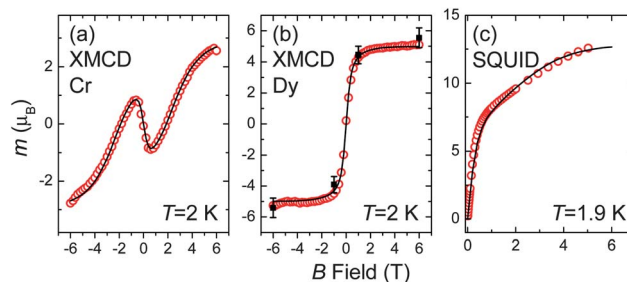


Fig. 4 Element-specific magnetisation curves of **1** for Cr (a) and Dy (b) measured at $T = 2$ K (red open circles). Black squares correspond to the total (spin and orbital) Dy magnetic moments obtained from sum rules at the respective fields. (c) Cluster magnetisation curve (red open circles) measured on **1** with SQUID magnetometry. Solid lines in (a,b,c) are the best-fit curves using Hamiltonian eqn (2).

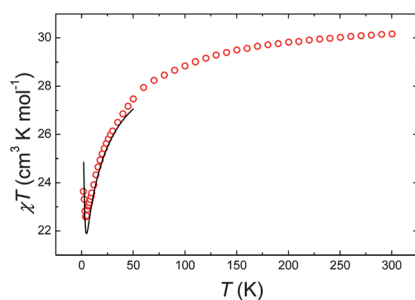


Fig. 5 Dc magnetic susceptibility of **1** (shown as the χT product, red open circles). The solid line shows the best fit using Hamiltonian eqn (1). We show this curve only up to 50 K, since the approximations of model eqn (1) do not hold beyond this temperature as discussed in the text.

the concomitant decrease in $\chi'(T)$ (see Fig. S4, ESI†) qualifies **1** as a SMM.

Muon-spin relaxation

To study the magnetisation dynamics of **1** at much shorter timescales than possible with our SQUID magnetometer we performed μ SR experiments. The muons are used as local probes of magnetic fields originating from the different magnetic ions in the cluster. The μ SR technique is sensitive to magnetic field fluctuations on timescales of $\sim 10^{-4}$ – 10^{-11} s, hence it covers a unique range of spin dynamics.²⁵ The temperature dependence of the magnetisation relaxation time displays Arrhenius behaviour as shown in Fig. 6b suggesting thermally-activated relaxation. From the fit a barrier of $\Delta_{\text{eff}} = 3.0(2)$ cm^{-1} and a preexponential factor of $\tau_0 = 5.3(4) \times 10^{-8}$ s are obtained. The small effective barrier readily explains the absence of a hysteresis and why no maximum in the out-of-phase ac susceptibility was observed in the accessible frequency and temperature range.

Inelastic neutron scattering

Fig. 7a and 7b show the powder INS spectra obtained on **1** for the indicated wavelengths and temperatures. The data were summed over the $|\mathbf{Q}|$ range from 0.9 to 1.8 \AA^{-1} . In the high-energy measurements shown in Fig. 7a, a single magnetic feature is

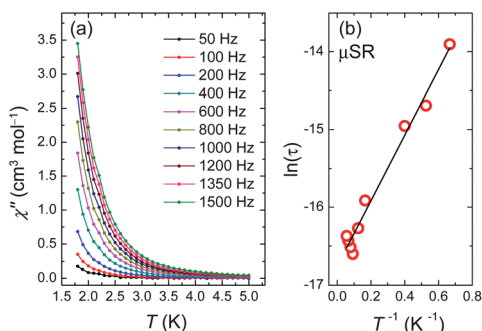


Fig. 6 (a) Out-of-phase component of the ac susceptibility (χ'') of **1** as a function of temperature at selected frequencies of the oscillating magnetic field obtained with $H_{\text{dc}} = 50$ mT. (b) Arrhenius plot of the magnetisation relaxation time of **1** measured by μ SR (red open circles) at zero magnetic field. The solid line is a fit to the Arrhenius law, yielding a barrier of $\Delta_{\text{eff}} = 3.0(2)$ cm^{-1} and a prefactor of $\tau_0 = 5.3(4) \times 10^{-8}$ s.

detected (peak I). The higher-resolution spectra shown in Fig. 7b reveal a three-fold splitting of peak I. All sub-peaks are of magnetic origin and can be attributed to transitions in the level scheme indicated in the inset of Fig. 7b. Details are given in the ESI†.

Spin-Hamiltonian models

In order to extract quantitative information and to gain a deeper understanding of our data we have employed spin-Hamiltonian models. According to Hund's rules the ground state of the free Dy^{III} ion is ${}^6\text{H}_{15/2}$. As a consequence of spin-orbit coupling, the first excited multiplet ${}^6\text{H}_{13/2}$ lies about 4000 cm^{-1} higher in energy.²⁶ Furthermore, in the presence of a ligand field the ground multiplet splits into eight Kramers doublets over an energy scale of typically hundreds of wave numbers,²⁷ and depending on the exact nature of the ligand field different ground state doublets (e.g. $\pm 15/2$, $\pm 13/2$) have been reported.¹¹ The experimental determination of the ground-state doublet from powder magnetization and susceptibility measurements can be problematic in 4f-containing clusters, in particular, when the symmetry of the ligand field is low. It has been shown recently that *ab initio* calculations can give insight here.²⁸

As a compromise between efficient calculations and reproduction of a maximum of the experimental data we use a Hamiltonian which operates in the restricted space of the ground state and the first-excited state Kramers doublets of each of the three ions. This *excited-state (encompassing) Hamiltonian* takes the form

$$\hat{H} = -j_{12}\hat{\mathbf{J}}_1 \cdot \hat{\mathbf{S}}_2 - j_{23}\hat{\mathbf{S}}_2 \cdot \hat{\mathbf{J}}_3 - j_{13}\hat{\mathbf{J}}_1 \cdot \hat{\mathbf{J}}_3 + \sum_i \left[D_i \left(\hat{S}_{iz}^2 - \frac{1}{3}S_i(S_i + 1) \right) + d_i \right] + \mu_B \sum_{i=1,3} g_i \hat{\mathbf{J}}_i \cdot \mathbf{B} + \mu_B g_2 \hat{\mathbf{S}}_2 \cdot \mathbf{B} \quad (1)$$

The first two terms represent isotropic nearest-neighbour exchange couplings, and the third term is a much weaker

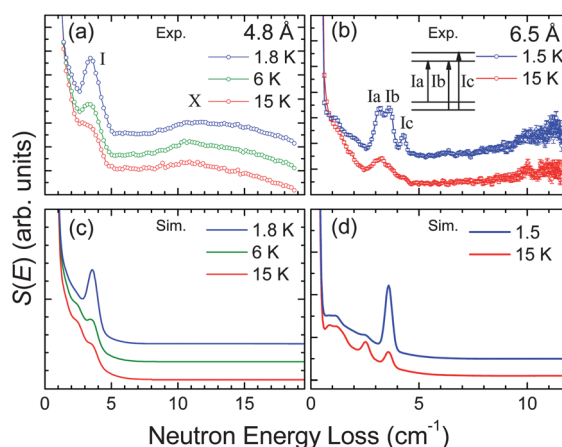


Fig. 7 (a, b) Inelastic neutron scattering spectra of **1** taken at the indicated wavelengths and temperatures. The intensity was summed over the useable $|\mathbf{Q}|$ range. The curves were offset to improve visibility. Error bars in (a) are smaller than the symbols. Inset in (b): level scheme obtained from the peak positions and the temperature dependence of the fine structure in (b). (c, d) Simulated INS spectra using eqn (1) with the best-fit parameters given in the text.

coupling between the Dy^{III} ions. At first sight the fourth anisotropy term describing the single-ion anisotropies seems unusual, but the proper choice of D_1 , D_3 , d_1 and d_3 simply generates splittings δ_1 and δ_3 between ground-state and first-excited-state doublets for the Dy^{III} ions.²⁹ In the fitting process it was found that the excited doublet of Dy(3) was not necessary to reproduce the experimental results; consequently it was neglected. For the Cr^{III} ion d_2 has to be zero. At low temperatures eqn (1) is an excellent approximation because of the large 4f-anisotropy splittings mentioned earlier. However, this approximation only holds as long as the population of energy levels higher than the first-excited doublet is negligible (see below). A similar model has been successfully applied in the case of a Dy₃ triangle.³⁰

The model can be made more effective, when considering the ground-state Kramers doublets only. In this simplest and widely used³¹ model the Dy^{III} ions are described by an effective angular momentum or pseudospin $S_1 = S_3 = 1/2$. The corresponding spin-1/2 Hamiltonian reads

$$\hat{H} = - \sum_{i < k} \hat{S}_i \cdot \mathbf{j}_{ik,\text{eff}} \cdot \hat{S}_k + D_2 \left[\hat{S}_{2,z}^2 - \frac{1}{3} S_2(S_2 + 1) \right] + \mu_B \sum_i \hat{S}_i \cdot \mathbf{g}_{i,\text{eff}} \cdot \mathbf{B}. \quad (2)$$

Obviously, ligand-field (anisotropic) terms are meaningless for a spin-1/2 system, hence only the Cr anisotropy remains here. However, it is important to note that the anisotropy of the Dy^{III} ions is now contained in the $\mathbf{j}_{ik,\text{eff}}$ and $\mathbf{g}_{i,\text{eff}}$ matrices with diagonal entries $\{j_{ik,\text{eff},xy}; j_{ik,\text{eff},xy}; j_{ik,\text{eff},z}\}$ and similar for $\mathbf{g}_{i,\text{eff}}$. For simplicity, in both models, eqn (1) and (2), it was assumed that all main anisotropy axes are collinear (along z). Details of the Hamiltonians and their interrelationship are discussed in the ESI†.

When comparing Hamiltonians eqn (1) and (2) it becomes obvious that the anisotropic exchange interaction in the spin-1/2 Hamiltonian is a consequence of the formalism when descending from the excited-state Hamiltonian to the spin-1/2 Hamiltonian. In other words, an isotropic exchange coupling in the excited-state Hamiltonian together with the strong 4f anisotropy leads to an anisotropic exchange coupling in the spin-1/2 Hamiltonian. It is, however, not possible to perform this reasoning in the backward sense: if an anisotropic exchange interaction is observed in an effective spin-1/2 model, it is not clear *a priori*, whether this interaction will be isotropic or not in the excited-state Hamiltonian.

Fits using the spin-1/2 Hamiltonian

The spin-1/2 Hamiltonian eqn (2) was least-squares fitted to the experimental Cr and Dy element-specific magnetisation curves and, simultaneously, to the cluster magnetisation curves obtained by SQUID measurements. Here, both Dy centres were treated identically, $\mathbf{g}_{13,\text{eff}} = \mathbf{g}_{1,\text{eff}} = \mathbf{g}_{3,\text{eff}}$, $\mathbf{j}_{\text{eff}} = \mathbf{j}_{12,\text{eff}} = \mathbf{j}_{23,\text{eff}}$, and $\mathbf{j}_{13,\text{eff}}$ and D_2 were set to zero to avoid overparameterisation. It was impossible to obtain a good fit with an Ising-only system, *i.e.* with $g_{13,\text{eff},xy} = 0$, $j_{\text{eff},xy} = 0 \text{ cm}^{-1}$ and $g_{13,\text{eff},z}$ and $j_{\text{eff},z}$ free to vary. In contrast, when $g_{13,\text{eff},xy}$ and $j_{\text{eff},xy}$ were allowed to assume nonzero values, the data could be excellently reproduced. The best-fit curves are shown as black solid lines in Fig. 4. The

\mathbf{j} -matrix anisotropy was linked to that of the \mathbf{g} -matrix using eqn (S5a)†. The best-fit parameters are

$$\begin{aligned} g_{13,\text{eff},xy} &= 5.7(5) \text{ (free)} \\ g_{13,\text{eff},z} &= 16.3(4) \text{ (free)} \\ j_{\text{eff},z} &= -2.8(1) \text{ cm}^{-1} \text{ (free)} \\ j_{\text{eff},xy} &= -0.98 \text{ cm}^{-1} \text{ (calculated from free parameters with eqn (S5a)†)}. \end{aligned}$$

Clearly, $g_{13,\text{eff},z}$ is less than 20.0 which would correspond to a $m_{13,\text{GS}} = \pm 15/2$ ground-state doublet. Hence, this result indicates that the ground-state doublets are characterised by $|m_{13,\text{GS}}| < 15/2$ and/or there is significant admixture of doublets because of non-uniaxial terms, not taken into account in Hamiltonians 1 and 2. Model eqn (2) obviously works in an excellent manner for reproducing all magnetisation data. However, by construction it is only valid at low temperatures and, in addition, the Dy \mathbf{g}_{eff} -matrices and exchange couplings $\mathbf{j}_{ik,\text{eff}}$ are effective quantities. This means that the magnetic parameters in eqn (2) that would allow for the comparison to theoretical values or other models are somewhat hidden.

Fits using the excited-state Hamiltonian

To improve the modelling, the first excited Kramers doublets are also taken into account using the excited-state Hamiltonian eqn (1). In the following we will show that this model is consistent with all our measurements on **1**. We have performed simultaneous least-squares fits of the excited-state Hamiltonian eqn (1) to the element-specific and cluster magnetisation obtained from XMCD and SQUID, respectively, as well as to the dc susceptibility. The separation of the excited state of Dy(1) was fixed to $\delta_1 = 53 \text{ cm}^{-1}$ by choosing D_1 and d_1 accordingly and a minor uniaxial anisotropy on the Cr site $D_2 = -0.52 \text{ cm}^{-1}$ (fixed) was introduced to simultaneously match the INS data, for reasons detailed below. The Cr g -factor was fixed to $g_S = 2$. The only fully independent parameters in this fit were the isotropic exchange couplings $j = j_{12} = j_{23}$ and j_{13} and the isotropic Dy g -factors $g_{13} = g_1 = g_3$. When both Dy^{III} centres were treated identically, no good fit could be obtained. Therefore, we tried different combinations of $\pm 11/2$, $\pm 13/2$, and $\pm 15/2$ ground and excited states by fixing the ground and excited-state doublets and determining the best-fit values. We found best agreement with the data when the ground state of Dy(1) was $m_{1,\text{GS}} = \pm 13/2$, its excited state was $m_{1,\text{ES}} = \pm 15/2$ and the ground state of Dy(3) was $m_{3,\text{GS}} = \pm 15/2$. When the ground-state $|m_{i,\text{GS}}|$ of at least one of the Dy ions was less than $13/2$, the calculated dc susceptibility was too low compared to the measured one. Also, adding the first-excited state of Dy(3) did not improve the fits. Therefore, only the ground-state doublet of Dy(3) was taken into account. The corresponding scenario is sketched in Fig. 8a.

The best-fit parameters are:

$$\begin{aligned} \delta_1 &= 53.0 \text{ cm}^{-1} \text{ (fixed)} \\ D_2 &= -0.52 \text{ cm}^{-1} \text{ (fixed)} \\ j_{12} = j_{23} &= -0.18(3) \text{ cm}^{-1} \text{ (free)} \\ j_{13} &= -0.011(4) \text{ cm}^{-1} \text{ (free)} \\ g_{13} &= 1.39(5) \text{ (free)}. \end{aligned}$$

Here, the extracted g -factor g_{13} is consistent with the value of $g_J = 4/3$. The Dy–Cr exchange coupling is rather weak, but very typical for 3d–4f clusters. Further, the coupling strength between Dy ions j_{13} is close to what is expected from through-space

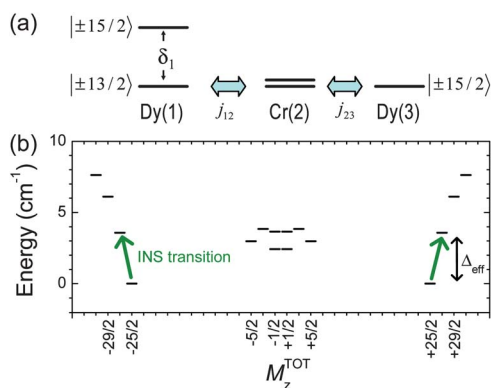


Fig. 8 (a) Scheme of the single-ion energy levels involved in the simulations using the excited-state Hamiltonian eqn (1). (b) Diagram depicting the lowest energy levels of **1** obtained by full diagonalisation of the excited-state Hamiltonian eqn (1) using the best-fit parameters given in the text. The value of the total M_z quantum number is used as x -axis. INS transitions are indicated as green arrows and the effective energy barrier from μ SR measurements is shown as a black arrow.

interaction. The calculated χT product using these parameters is drawn as a solid black line in Fig. 5. The simulated INS spectra are shown in Fig. 7c and 7d, demonstrating excellent agreement with the experimental data.

When performing the INS simulations we noticed that a small uniaxial anisotropy on the Cr site of $D_2 = -0.52 \text{ cm}^{-1}$ was necessary to accurately match both INS and XMCD results simultaneously. D_2 mainly leads to a small shift of the INS feature I towards higher energy transfers. Furthermore, we observed that a strong INS transition appears at an energy transfer approximately equal to the separation δ_1 . As the fitting results improved with decreasing δ_1 , but no strong, magnetic INS transition other than INS peak I was observed, we fixed the separation to $\delta_1 = 53.0 \text{ cm}^{-1}$ which is a value higher than the maximum energy loss of all our INS data. Whereas the high-energy measurements are excellently reproduced, the fine structure observed in Fig. 7b is not captured in full detail. As indicated earlier in the text, the fine structure splitting is in the sub-Kelvin range, implying that it is caused by very weak effects. The introduction of a biaxial anisotropy on the Cr^{III} site or the consideration of unequal exchange couplings $j_{12} \neq j_{23}$ did not allow us to satisfactorily reproduce this fine structure. A possible source of the fine structure could be a non-collinear arrangement of the main anisotropy axes of the three ions. However, although these fine details could not be fully reproduced, certainly the major terms that govern the magnetism of **1** are implemented in our model.

As a result of the restricted basis set, the spectrum of the excited-state Hamiltonian ends at an energy of $\sim 60 \text{ cm}^{-1}$. Any possible higher-energy levels are not taken into account implying that accurate results can be obtained with Hamiltonian eqn (1) for temperatures lower than $\sim 50 \text{ K}$. This is clearly visible in the fit to the dc magnetic susceptibility in Fig. 5.

Density-functional theory

Density-functional theory (DFT) and quantum chemical calculations of 3d–4f systems have been reported on Gd^{III}–M(3d)

dimers,^{28a,32} whereas the present study is, to the best of our knowledge, the first reporting a DFT calculation on a 3d–4f molecular cluster with a nonzero orbital momentum ground state.

Geometrical optimisation of the truncated model cluster on the (Perdew–Wang) GGA level in scalar-relativistic approximation using a planewave pseudopotential approach³³ well reproduces the molecular structure (for details see ESI†). The GGA-predicted ground-state spin values are $S = 3/2$ (Cr) and $S = 5/2$ (Dy), the latter value is consistent with what is expected for a Dy^{III} ion. A value for the orbital angular momentum is not provided in the scalar-relativistic approximation. Using a scalar-relativistic atom-centred localized basis set approach with a modern hybrid functional (M06-2X),³⁴ a spin magnetic moment of the Cr^{III} ion of $-3.0 \mu_B$ is obtained which is aligned antiparallel to the Dy spin moment of $5.0 \mu_B$. This ferrimagnetic state is consistent with the XMCD measurements at low magnetic fields. The computed exchange coupling is $j = -40.83 \text{ cm}^{-1}$ with the Ginsberg–Noodleman–Davidson expression³⁵ and -32.66 cm^{-1} with the expression of Ruiz *et al.*³⁶ for the experimental crystal structure. Details about the calculations can be found in the ESI†. Note that the mapping of the DFT calculations to the spin Hamiltonian is based on spin-only values S^2 or $S(S + 1)$ (see ESI†). Obviously, the DFT calculations overestimate the exchange coupling. This could be related to a spurious influence of the self-interaction error which will make the Dy 4f orbitals less localised, or it could be related to an influence of the spin-orbit interaction.

The hybrid-functional computed spin densities and the spin polarisation for the ferromagnetic state of the truncated structure are shown in Fig. 9. Here, significant spin polarisation is seen on the magnetic ions but there is also some on the O ligands of Dy, the N ligands of Cr and the bridging fluoride. Importantly, the alternating positive/negative spin polarisation on the latter indicates superexchange interaction. Further, the polarisation of the Cr^{III} ion creates opposite, induced polarisation on its N ligands. In contrast, the parallel orientation of the Dy–O polarization can only be explained by a charge delocalization from Dy to O.

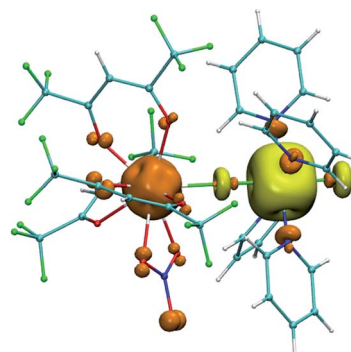


Fig. 9 Spin-density isosurface computed for the zero-field antiferromagnetic state of the truncated model cluster as described in the text. Positive (negative) spin polarisation is plotted as orange (yellow) color. Note that the alternating spin polarisation on the bridging fluoride ion is typical for superexchange.

Discussion

From the element-specific magnetisation curves obtained from XMCD as shown in Fig. 4a and 4b the arrangement of the magnetic moments can be directly read off: Obviously the Dy magnetic moments are close to saturation at a field of $B = 1$ T, indicating a large magnetic moment which is aligned parallel to the applied magnetic field. This is what is expected. In stark contrast, the Cr magnetisation curve exhibits a pronounced wiggle shape with a triple-zero crossing, and only at high magnetic fields it shows the onset of saturation, close to a value of $m_{\text{sat,Cr}} = 3 \mu_{\text{B}}$ consistent with $S_2 = 3/2$ and $g_S = 2$. The wiggle shape implies that at low magnetic fields, the Cr moment is aligned antiparallel to the field and thus to the Dy moments. This behaviour results from the weak antiferromagnetic coupling between the Dy^{III} and Cr^{III} ions observed in **1**: At low magnetic fields it is energetically favourable for the total cluster to assume a ferrimagnetic spin alignment, whereas at high magnetic fields the Zeeman energy overcomes the exchange-coupling energy and the total-cluster energy can be minimised by reversing the Cr spin, leading to a ferromagnetic configuration.

To illustrate the underlying effect of the weak exchange coupling we have performed simulations using the effective spin-1/2 Hamiltonian eqn (2). Here, the Dy^{III} ions were treated identically, $\mathbf{g}_{13,\text{eff}} = \mathbf{g}_{1,\text{eff}} = \mathbf{g}_{3,\text{eff}}$, $\mathbf{j}_{\text{eff}} = \mathbf{j}_{12,\text{eff}} = \mathbf{j}_{23,\text{eff}}$, and $\mathbf{j}_{13,\text{eff}} = 0$. The simplified assumptions were $g_{13,\text{eff},xy} = 0$ and $j_{\text{eff},xy} = 0 \text{ cm}^{-1}$, and the z -components of the Dy \mathbf{g}_{eff} matrices were $g_{13,\text{eff},z} = 20.0$, implying a ground-state Kramers doublet of $m_{13,\text{GS}} = \pm 15/2$. The results for different values of $j_{\text{eff},z}$ are shown in Fig. 10. While the Dy magnetisation curves are only weakly dependent on the choice of $j_{\text{eff},z}$, the Cr magnetisation is dramatically affected, delivering a good measure of the exchange coupling.

In addition, we observed that indeed a quite accurate value of the exchange coupling $j = j_{12} = j_{23}$ in the more complex Hamiltonian eqn (1) can be deduced from the simple relation $j_{12} = j_{12,\text{eff},z} g/g_{13,\text{eff},z}$ obtained from eqn (S5b) and (S5c)†. Using the effective values $j_{12,\text{eff},z}$ and $g_{13,\text{eff},z}$ obtained from the spin-1/2 Hamiltonian fits to the magnetisation curves, we calculate the non-effective exchange coupling (in Hamiltonian eqn (1)) to be $j_{12} = -0.23 \text{ cm}^{-1}$. This value is very close to that found by the more detailed analysis involving INS and dc magnetic susceptibility suggesting that XMCD data alone can provide sufficient experimental evidence for the extraction of the Dy–Cr exchange coupling in simple clusters. The further agreement with INS and SQUID results underline the strength of the modelling.

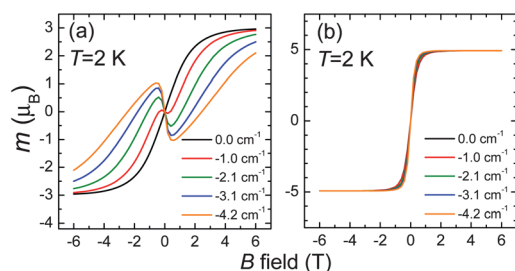


Fig. 10 Simulation of the element-specific magnetisation curves of Cr (a) and Dy (b) using the effective spin-1/2 Hamiltonian eqn (2) with different coupling strengths $j_{\text{eff},z}$ as indicated in the plots. Other parameters are given in the text.

The INS and μSR results can be further understood by using the low-energy spectrum plotted in Fig. 8b. Here, the total-spin m_s value $M_z^{\text{TOT}} = \langle m | \sum \hat{S}_{i,z} | m \rangle$ is used as x -axis. The spectrum was obtained by full diagonalisation of the excited-state Hamiltonian eqn (1) using the best-fit parameters. The ground states are characterised by a $|\pm 25/2\rangle$ doublet reflecting the ferrimagnetic arrangement of the Dy and Cr magnetic moments. The INS transition I is indicated by green arrows and a black arrow shows the height of the effective energy barrier of $\Delta_{\text{eff}} = 3.0 \text{ cm}^{-1}$ obtained by μSR . This barrier height can be explained by considering small non-uniaxial terms in the excited-state Hamiltonian. In the simplest case, this could be a cluster E (biaxial anisotropy) term. In general, such a term is able to mix energy eigenstates with $\Delta M_z^{\text{TOT}} = \pm 2k$ with integer k , and regarding the spectrum of **1** it would be weakly allowed that the $|\pm 25/2\rangle$ ground states mix with the excited $|\mp 27/2\rangle$ states located at an energy of 3.6 cm^{-1} . Such a mixing would give rise to quantum tunnelling of the magnetisation through the excited states, explaining the observed temperature dependence of the relaxation time and the low effective barrier for magnetization reversal.

As aforementioned, the DFT calculations are successful in reproducing the molecular geometry of the truncated model system and the sign of the magnetic exchange coupling. Fig. 9 reveals that the bridging fluoride ion which mediates the Dy–Cr interaction is spin-polarised in an alternating positive/negative fashion substantiating that superexchange is at the origin of the antiferromagnetic exchange coupling. Although the ligand spin polarisation may appear large in the spin-polarisation map, it is only on the order of $0.03 \mu_{\text{B}}$. Therefore it is justified to neglect it in the spin-Hamiltonian analysis.

Conclusions

We have reported the syntheses and crystal structures of two novel 3d–4f clusters containing Dy and Cr featuring linear, unsupported fluoride bridges. Further, we have performed an in-depth study of the magnetism of the trinuclear compound **1**. The element-specific magnetisation curves obtained from XMCD directly reveal the field-induced transition from the ferrimagnetic to the ferromagnetic alignments of the Dy and Cr magnetic moments. Our findings are corroborated by SQUID magnetometry and INS which confirm the isotropic Dy–Cr exchange coupling of $j = -0.18 \text{ cm}^{-1}$ obtained from XMCD. The μSR and ac susceptibility measurements suggest that **1** is a SMM with a small effective barrier $\Delta_{\text{eff}} = 3 \text{ cm}^{-1}$. We have successfully modelled the data using spin-Hamiltonian models at different levels of complexity. The DFT calculations reveal spin polarisation on the Dy and Cr ligands and suggest that the antiferromagnetic Dy–Cr coupling originates from superexchange *via* the fluoride ion bridge.

Our results demonstrate that XMCD is suitable to determine the sign and strength of the weak exchange coupling between Dy and Cr ions. This mitigates the problem that in such 3d–4f compounds often the information about intracluster magnetic couplings contained in the temperature-dependent magnetic susceptibility is concealed by the much stronger effect of the 4f-anisotropy splittings. As this scenario can be expected to be

realised in most 3d–4f compounds, our approach may be applicable to a large number of oligonuclear 3d–4f compounds.

Notes and references

- (a) A. Caneschi, D. Gatteschi, R. Sessoli, A. L. Barra, L. C. Brunel and M. Guillot, *J. Am. Chem. Soc.*, 1991, **113**, 5873; (b) R. Sessoli, D. Gatteschi, A. Caneschi and M. A. Novak, *Nature*, 1993, **365**, 141; (c) D. Gatteschi, A. Caneschi, L. Pardi and R. Sessoli, *Science*, 1994, **265**, 1054; (d) G. Christou, D. Gatteschi, D. N. Hendrickson and R. Sessoli, *MRS Bull.*, 2000, **25**, 66; (e) C. Cadiou, M. Murrie, C. Paulsen, V. Villar, W. Wernsdorfer and R. E. P. Winpenny, *Chem. Commun.*, 2001, 2666; (f) J. J. Sokol, A. G. Hee and J. R. Long, *J. Am. Chem. Soc.*, 2002, **124**, 7656; (g) C. J. Milios, A. Vinslava, W. Wernsdorfer, S. Moggach, S. Parsons, S. P. Perlepes, G. Christou and E. K. Brechin, *J. Am. Chem. Soc.*, 2007, **129**, 2754.
- (a) O. Waldmann, *Inorg. Chem.*, 2007, **46**, 10035; (b) E. Ruiz, J. Cirera, J. Cano, S. Alvarez, C. Loose and J. Kortus, *Chem. Commun.*, 2008, 52; (c) R. Sessoli and A. K. Powell, *Coord. Chem. Rev.*, 2009, **253**, 2328; (d) L. Sorace, C. Benelli and D. Gatteschi, *Chem. Soc. Rev.*, 2011, **40**, 3092.
- (a) N. Ishikawa, M. Sugita, T. Ishikawa, S. Koshihara and Y. Kaizu, *J. Am. Chem. Soc.*, 2003, **125**, 8694; (b) N. Ishikawa, *Polyhedron*, 2007, **26**, 2147.
- (a) M. A. Aldamen, J. M. Clemente-Juan, E. Coronado, C. Marti-Gastaldo and A. Gaita-Arino, *J. Am. Chem. Soc.*, 2008, **130**, 8874; (b) M. A. Aldamen, S. Cardona-Serra, J. M. Clemente-Juan, E. Coronado, A. Gaita-Arino, C. Marti-Gastaldo, F. Luis and O. Montero, *Inorg. Chem.*, 2009, **48**, 3467.
- S.-D. Jiang, B.-W. Wang, H.-L. Sun, Z.-M. Wang and S. Gao, *J. Am. Chem. Soc.*, 2011, **133**, 4730.
- R. Giraud, W. Wernsdorfer, A. M. Tkachuk, D. Mailly and B. Barbara, *Phys. Rev. Lett.*, 2001, **87**, 057203.
- (a) P.-H. Lin, T. Burchell, L. Ungur, L. Chibotaru, W. Wernsdorfer and M. Murugesu, *Angew. Chem., Int. Ed.*, 2009, **48**, 9489; (b) I. J. Hewitt, J. Tang, N. T. Madhu, C. E. Anson, Y. Lan, J. Luzon, M. Etienne, R. Sessoli and A. K. Powell, *Angew. Chem., Int. Ed.*, 2010, **49**, 6352; (c) Y.-N. Guo, G.-F. Xu, P. Gamez, L. Zhao, S.-Y. Lin, R. Deng, J. Tang and H.-J. Zhang, *J. Am. Chem. Soc.*, 2010, **132**, 8538; (d) R. J. Blagg, C. A. Muryn, E. J. L. McInnes, F. Tuna and R. E. P. Winpenny, *Angew. Chem., Int. Ed.*, 2011, **50**, 6530; (e) J. Long, F. Habib, P.-H. Lin, I. Korobkov, G. Enright, L. Ungur, W. Wernsdorfer, L. F. Chibotaru and M. Murugesu, *J. Am. Chem. Soc.*, 2011, **133**, 5319.
- (a) J. D. Rinehart, M. Fang, W. J. Evans and J. R. Long, *Nat. Chem.*, 2011, **3**, 538; (b) J. D. Rinehart, M. Fang, W. J. Evans and J. R. Long, *J. Am. Chem. Soc.*, 2011, **133**, 14236.
- (a) C. M. Zaleski, E. C. Deppner, J. W. Kampf, M. L. Kirk and V. L. Pecoraro, *Angew. Chem., Int. Ed.*, 2003, **43**, 3912; (b) S. Osa, T. Kido, N. Matsumoto, N. Re, A. Pochaba and J. Mrozinski, *J. Am. Chem. Soc.*, 2004, **126**, 420; (c) A. Mishra, W. Wernsdorfer, K. A. Abboud and G. Christou, *J. Am. Chem. Soc.*, 2004, **126**, 15648; (d) F. Mori, T. Ishida and T. Nogami, *Polyhedron*, 2005, **24**, 2588; (e) J. P. Costes, F. Dahan and W. Wernsdorfer, *Inorg. Chem.*, 2006, **45**, 5; (f) C. Aronica, G. Pilet, G. Chastanet, W. Wernsdorfer, J. F. Jacquot and D. Luneau, *Angew. Chem., Int. Ed.*, 2006, **45**, 4659; (g) V. Mereacre, A. M. Ako, R. Clerac, W. Wernsdorfer, I. J. Hewitt, C. E. Anson and A. K. Powell, *Chem.–Eur. J.*, 2008, **14**, 3577; (h) J. Rinck, G. Novitchi, W. Van den Heuvel, L. Ungur, Y. Lan, W. Wernsdorfer, C. E. Anson, L. F. Chibotaru and A. K. Powell, *Angew. Chem., Int. Ed.*, 2010, **49**, 7583; (i) M. Holyńska, D. Premuzić, I.-R. Jeon, W. Wernsdorfer, R. Clérac and S. Dehnen, *Chem.–Eur. J.*, 2011, **17**, 9605.
- W. W. Lukens and M. D. Walter, *Inorg. Chem.*, 2010, **49**, 4458.
- (a) N. Ishikawa, M. Sugita, T. Okubo, N. Tanaka, T. Iino and Y. Kaizu, *Inorg. Chem.*, 2003, **42**, 2440; (b) J. Luzon, K. Bernot, I. J. Hewitt, C. E. Anson, A. K. Powell and R. Sessoli, *Phys. Rev. Lett.*, 2008, **100**, 247205.
- (a) G. van der Laan and B. T. Thole, *Phys. Rev. B: Condens. Matter*, 1991, **43**, 13401; (b) J. Stöhr, *J. Magn. Magn. Mater.*, 1999, **200**, 470; (c) T. Funk, A. Deb, S. J. George, H. Wang and S. P. Cramer, *Coord. Chem. Rev.*, 2005, **249**, 3.
- (a) M.-A. Arrio, A. Sculler, P. Sainctavit, C. Cartier dit Moulin, T. Mallah and M. Verdager, *J. Am. Chem. Soc.*, 1999, **121**, 6414; (b) G. Champion, N. Lalioi, V. Tangoulis, M.-A. Arrio, P. Sainctavit, F. Villain, A. Caneschi, D. Gatteschi, C. Giorgetti, F. Baudelet, M. Verdager and C. Cartier dit Moulin, *J. Am. Chem. Soc.*, 2003, **125**, 8371; (c) R. Moroni, C. Cartier dit Moulin, G. Champion, M.-A. Arrio, P. Sainctavit, M. Verdager and D. Gatteschi, *Phys. Rev. B: Condens. Matter*, 2003, **68**, 064407; (d) T. Hamamatsu, K. Yabe, M. Towatari, S. Osa, N. Matsumoto, N. Re, A. Pochaba, J. Mrozinski, J. L. Gallani, A. Barla, P. Imperia, C. Paulsen and J. P. Kappler, *Inorg. Chem.*, 2007, **46**, 4458; (e) M. Mannini, F. Pineider, P. Sainctavit, C. Danieli, E. Otero, C. Sciancalepore, A. M. Talarico, M.-A. Arrio, A. Cornia, D. Gatteschi and R. Sessoli, *Nat. Mater.*, 2009, **8**, 194; (f) G. Rogez, B. Donnio, E. Terazzi, J.-L. Gallani, J.-P. Kappler, J.-P. Bucher and M. Drillon, *Adv. Mater.*, 2009, **21**, 4323; (g) P. Gambardella, S. Stepanow, A. Dmitriev, J. Honolka, F. M. F. de Groot, M. Lingenfelder, S. Sen Gupta, D. D. Sarma, P. Bencok, S. Stanescu, S. Clair, S. Pons, N. Lin, A. P. Seitsonen, H. Brune, J. V. Barth and K. Kern, *Nat. Mater.*, 2009, **8**, 189; (h) R. Biagi, J. Fernandez-Rodriguez, M. Gonidec, A. Mironne, V. Corradini, F. Moro, V. De Renzi, U. del Pennino, J. C. Cezar, D. B. Amabilino and J. Veciana, *Phys. Rev. B: Condens. Matter Phys.*, 2010, **82**, 224406; (i) S. Stepanow, J. Honolka, P. Gambardella, L. Vitali, N. Abdurakhmanova, T.-C. Tseng, S. Rauschenbach, S. L. Tait, V. Sessi, S. Klyatskaya, M. Ruben and K. Kern, *J. Am. Chem. Soc.*, 2010, **132**, 11900; (j) M. Prinz, K. Kuepper, C. Taubitz, M. Raekers, S. Khanra, B. Biswas, T. Weyhermüller, M. Uhlarz, J. Wosniza, J. Schnack, A. V. Postnikov, C. Schröder, S. J. George, M. Neumann and P. Chaudhuri, *Inorg. Chem.*, 2010, **49**, 2093; (k) V. Corradini, A. Ghirri, U. del Pennino, R. Biagi, V. A. Milway, G. Timco, F. Tuna, R. E. P. Winpenny and M. Affronte, *Dalton Trans.*, 2010, **39**, 4928; (l) M. Gonidec, R. Biagi, V. Corradini, F. Moro, V. De Renzi, U. del Pennino, D. Summa, L. Muccioli, C. Zannoni, D. B. Amabilino and J. Veciana, *J. Am. Chem. Soc.*, 2011, **133**, 6603; (m) M. Mannini, E. Tancini, L. Sorace, P. Sainctavit, M.-A. Arrio, Y. Qian, E. Otero, D. Chiappe, L. Margheriti, J. C. Cezar, R. Sessoli and A. Cornia, *Inorg. Chem.*, 2011, **50**, 2911; (n) A. Lodi Rizzini, C. Krull, T. Balashov, J. J. Kavich, A. Mugarza, P. S. Miedema, P. K. Thakur, V. Sessi, S. Klyatskaya, M. Ruben, S. Stepanow and P. Gambardella, *Phys. Rev. Lett.*, 2011, **107**, 177205.
- (a) M. T. Gamer, Y. Lan, P. W. Roesky, A. K. Powell and R. Clérac, *Inorg. Chem.*, 2008, **47**, 6581; (b) R. Bircher, B. F. Abrahams, H. U. Güdel and C. Boskovic, *Polyhedron*, 2007, **26**, 3023; (c) L. G. Westin, M. Kristikos and A. Caneschi, *Chem. Commun.*, 2003, 1012; (d) T. Kajiwara, K. Katagiri, S. Takaishi, M. Yamashita and N. Iki, *Chem.–Asian J.*, 2006, **1**, 349.
- (a) F. Pointillart, K. Bernot and R. Sessoli, *Inorg. Chem. Commun.*, 2007, **10**, 471; (b) F. Pointillart, K. Bernot, R. Sessoli and D. Gatteschi, *Inorg. Chem.*, 2010, **49**, 4355; (c) P.-H. Lin, I. Korobkov, W. Wernsdorfer, L. Ungur, L. F. Chibotaru and M. Murugesu, *Eur. J. Inorg. Chem.*, 2011, 1535.
- (a) T. Birk, K. S. Pedersen, S. Piligkos, C. A. Thuesen, H. Weihe and J. Bendix, *Inorg. Chem.*, 2011, **50**, 5312; (b) T. Birk, M. J. Magnussen, S. Piligkos, H. Weihe, A. Holten and J. Bendix, *J. Fluorine Chem.*, 2010, **131**, 898.
- F. Perdih, A. Demsar, A. Pevec, S. Petricek, I. Leban, G. Giester, J. Sieler and H. W. Roesky, *Polyhedron*, 2001, **20**, 1967.
- A. Pevec, M. Mrak, A. Demsar, S. Petricek and H. W. Roesky, *Polyhedron*, 2003, **22**, 575.
- A. McRobbie, A. R. Sarwar, S. Yeninas, H. Nowell, M. L. Baker, D. Allan, M. Luban, C. A. Muryn, R. G. Pritchard, R. Prozorov, G. A. Timco, F. Tuna, G. F. S. Whitehead and R. E. P. Winpenny, *Chem. Commun.*, 2011, **47**, 6251.
- T. Birk, M. Schau-Magnussen, T. Weyhermüller and J. Bendix, *Acta Crystallogr., Sect. E: Struct. Rep. Online*, 2011, **67**, m1561.
- (a) J. Glerup, J. Josephsen, K. Michelsen, E. Pedersen and C. E. Schäffer, *Acta Chem. Scand.*, 1970, **24**, 247; (b) P. Andersen, A. Døssing, J. Glerup and M. Rude, *Acta Chem. Scand.*, 1990, **44**, 346; (c) A. Böttcher, H. Elias, J. Glerup, M. Neuburger, C. E. Olsen, H. Paulus, J. Springborg and M. Zehnder, *Acta Chem. Scand.*, 1994, **48**, 967; (d) A. Böttcher, H. Elias, J. Glerup, M. Neuburger, C. E. Olsen, J. Springborg, H. Weihe and M. Zehnder, *Acta Chem. Scand.*, 1994, **48**, 981.

- 22 G. Fochi, J. Strähle and F. Gingl, *Inorg. Chem.*, 1991, **30**, 4669.
- 23 (a) B. T. Thole, P. Carra, F. Sette and G. van der Laan, *Phys. Rev. Lett.*, 1992, **68**, 1943; (b) P. Carra, B. T. Thole, M. Altarelli and X. Wang, *Phys. Rev. Lett.*, 1993, **70**, 694; (c) C. T. Chen, Y. U. Idzerda, H.-J. Lin, N. V. Smith, G. Meigs, E. Chaban, G. H. Ho, E. Pellegrin and F. Sette, *Phys. Rev. Lett.*, 1995, **75**, 152.
- 24 (a) Y. Teramura, A. Tanaka and T. Jo, *J. Phys. Soc. Jpn.*, 1996, **65**, 1053; (b) C. Piamonteze, P. Miedema and F. M. F. de Groot, *Phys. Rev. B: Condens. Matter Mater. Phys.*, 2009, **80**, 184410.
- 25 (a) T. Lancaster, S. J. Blundell, F. L. Pratt, I. Franke, A. J. Steele, P. J. Baker, Z. Salman, C. Baines, I. Watanabe, S. Carretta, G. A. Timco and R. E. P. Winpenny, *Phys. Rev. B: Condens. Matter Mater. Phys.*, 2010, **81**, 140409; (b) Z. Salman, S. R. Giblin, Y. Lan, A. K. Powell, R. Scheuermann, R. Tingle and R. Sessoli, *Phys. Rev. B: Condens. Matter Mater. Phys.*, 2010, **82**, 174427.
- 26 S. Cotton, *Lanthanide and Actinide Chemistry*; John Wiley & Sons, 2006.
- 27 A. Abragam and B. Bleaney, *Electron Paramagnetic Resonance of Transition Metal Ions*; Dover: New York, 1986.
- 28 (a) J. Paulovic, F. Cimpoesu, M. Ferbinteanu and K. J. Hirao, *J. Am. Chem. Soc.*, 2004, **126**, 3321; (b) L. Chibotaru, L. Ungur and A. Soncini, *Angew. Chem., Int. Ed.*, 2008, **47**, 4126; (c) K. Bernot, J. Luzon, L. Bogani, M. Etienne, C. Sangregorio, M. Shanmugam, A. Caneschi, R. Sessoli and D. Gatteschi, *J. Am. Chem. Soc.*, 2009, **131**, 5573.
- 29 *E.g.*, a ground state of $m_i = \pm 15/2$ and a first excited state of $m_i = \pm 13/2$ generate $D_i = -\delta_i/14$ and $d_i = 2\delta_i$.
- 30 J. Luzon, K. Bernot, I. J. Hewitt, C. E. Anson, A. K. Powell and R. Sessoli, *Phys. Rev. Lett.*, 2008, **100**, 247205.
- 31 A. Palii, B. Tsukerblat, S. Klokishner, K. R. Dunbar, J. M. Clemente-Juan and E. Coronado, *Chem. Soc. Rev.*, 2011, **40**, 3130, and references therein.
- 32 (a) I. Rudra, C. Raghu and S. Ramasesha, *Phys. Rev. B: Condens. Matter*, 2002, **65**, 224411; (b) X.-R. Sun, Z.-D. Chen, M.-W. Wang, B.-W. Wang, F. Yan and K.-K. Cheung, *Chin. J. Chem.*, 2007, **25**, 329; (c) G. Rajaraman, F. Totti, A. Bencini, A. Caneschi, R. Sessoli and D. Gatteschi, *Dalton Trans.*, 2009, 3153.
- 33 (a) G. Kresse and J. Hafner, *Phys. Rev. B: Condens. Matter*, 1993, **47**, 558; (b) G. Kresse and J. Furthmüller, *Phys. Rev. B: Condens. Matter*, 1996, **54**, 11169; (c) P. E. Blöchl, *Phys. Rev. B: Condens. Matter*, 1994, **50**, 17953; (d) G. Kresse and J. Furthmüller, *Phys. Rev. B: Condens. Matter*, 1996, **54**, 11169.
- 34 Y. Zhao and D. Truhlar, *Theor. Chem. Acc.*, 2008, **120**, 215.
- 35 (a) A. P. Ginsberg, *J. Am. Chem. Soc.*, 1980, **102**, 111; (b) L. Noodleman, *J. Chem. Phys.*, 1981, **74**, 5737; (c) L. Noodleman and E. R. Davidson, *Chem. Phys.*, 1986, **109**, 131.
- 36 E. Ruiz, J. Cano, S. Alvarez and P. Alemany, *J. Comput. Chem.*, 1999, **20**, 1391.